Received: 28 May 2018 | Revised: 23 August 2018 | Accepted: 27 September 2018

DOI: 10.1002/pip.3085

RESEARCH ARTICLE

WILEY PROGRESS IN PHOTOVOLTAICS

Designing a hybrid thin-film/wafer silicon triple photovoltaic junction for solar water splitting

Paula Perez-Rodriguez[1] | Wouter Vijselaar[2] | Jurriaan Huskens[2] | Machiel Stam[1] | Michael Falkenberg[1,3] | Miro Zeman[1] | Wilson Smith[4] | Arno H.M. Smets[1]

[1] Photovoltaic Materials and Devices (PVMD) group, Delft University of Technology, Delft, The Netherlands

[2] Molecular NanoFabrication, MESA+ Institute for Nanotechnology, University of Twente, Enschede, The Netherlands

[3] Hamburg University of Applied Sciences, Hamburg, Germany

[4] Materials for Energy Storage and Conversion (MECS) group, Delft University of Technology, Delft, The Netherlands

Correspondence
Paula Perez-Rodriguez, Photovoltaic Materials and Devices (PVMD) group, Delft University of Technology, Mekelweg 4, Delft 2628 CD, The Netherlands.
Email: p.perezrodriguez@tudelft.nl

Funding information
Stichting voor Fundamenteel Onderzoek der Materie, Grant/Award Number: FOM-13CO19

Abstract

Solar fuels are a promising way to store solar energy seasonally. This paper proposes an earth-abundant heterostructure to split water using a photovoltaic-electrochemical device (PV-EC). The heterostructure is based on a hybrid architecture of a thin-film (TF) silicon tandem on top of a c-Si wafer (W) heterojunction solar cell (a-Si:H (TF)/nc-Si:H (TF)/c-Si(W)) The multijunction approach allows to reach enough photovoltage for water splitting, while maximizing the spectrum utilization. However, this unique approach also poses challenges, including the design of effective tunneling recombination junctions (TRJ) and the light management of the cell. Regarding the TRJs, the solar cell performance is improved by increasing the n-layer doping of the middle cell. The light management can be improved by using hydrogenated indium oxide (IOH) as transparent conductive oxide (TCO). Finally, other light management techniques such as substrate texturing or absorber bandgap engineering were applied to enhance the current density. A correlation was observed between improvements in light management by conventional surface texturing and a reduced nc-Si:H absorber material quality. The final cell developed in this work is a flat structure, using a top absorber layer consisting of a high bandgap a-Si:H. This triple junction cell achieved a PV efficiency of 10.57%, with a fill factor of 0.60, an open-circuit voltage of 2.03 V and a short-circuit current density of 8.65 mA/cm^2. When this cell was connected to an IrO_x/Pt electrolyser, a stable solar-to-hydrogen (STH) efficiency of 8.3% was achieved and maintained for 10 hours.

KEYWORDS

electrolysis, heterostructures, hydrogen fuel, multijunction, open-circuit voltage, photovoltaic

1 | INTRODUCTION

Because of the intermittent solar radiation availability, energy storage is a key factor for the implementation of solar energy. Chemical fuels such as hydrogen, carbohydrate, or ammonia are amongst the most feasible options, since they are highly energetic fuels that can be easily stored for long periods of time.[1] In particular, electrochemical (EC) splitting of water offers a promising way to convert solar energy into hydrogen because of its low conversion losses. Hydrogen production requires a thermodynamic EC voltage of 1.23 V. In addition, overpotentials are caused by the charge carrier transport in the electrodes and the electrolyte, catalytic effects, and other losses of the

systems.[2] As a result, the total voltage required to drive the reaction[3] is in the range from 1.6 to 2.0 V. There are several ways to achieve this voltage using semiconductor materials. To achieve a feasible design, the proposed device should use relatively stable and cheap material. Moreover, a recent study suggests that multijunction devices are preferred to achieve high efficiencies for water splitting applications. A material that combines these advantages is silicon. A possible approach to achieve the high voltages needed using silicon could be a novel multijunction consisting of a hybrid device that combines wafer (W) and thin-film (TF) silicon technologies. This concept has already been proven to be able to achieve high open circuit voltages and short circuit current densities in double junctions.[4] In the case of water splitting, an a-Si:H (TF)/nc-Si:H (TF)/c-Si(W) triple junction device has been proposed for solar water splitting, with a potential to achieve solar-to-hydrogen (STH) efficiencies[5] of about 9%. This approach is further explored in this paper.

The proposed hybrid device can provide high enough voltages for solar water splitting, with a considerable increase in current density due to better spectral utilization. However, there are also areas of optimization, including the tunneling recombination junctions (TRJ), the growth of high quality absorber layers on flat and textured surfaces, and the light management strategies.[6,7] This paper first analyses the TRJs between the different subcells, which were deposited on flat surface configuration to better recognize the electrical effects. A TRJ junction is expected to increase recombination from both sides of the junction to ensure current continuity. To achieve high recombination in a TRJ, the band alignment should be such that the conduction band of the n-side has an energy close to the p-side valence band to enhance tunneling. Water splitting applications are particularly sensitive to the values of open-circuit voltage (V_{oc}) and fill factor (*FF*), in which TRJs play a crucial role. The junction between the a-Si:H cell and the nc-Si:H cell have been previously studied.[8-10] However, the junction between the nc-Si:H cell and the silicon heterojunction (SHJ) cell is relatively unexplored.[11,12] Moreover, in order to improve the current density of the multijunction solar cell, light management techniques need to be implemented. First, conventional texturing of the crystalline silicon substrate was considered in order to increase the light absorption within the cell, exploring its light trapping capabilities and the adhesion, crystallinity, and material quality of the nc-Si:H absorber layer. Second, these multijunction cells tend to be limited by the middle cell, mainly due to the overlapping absorption between the top and middle cell. This paper explores the use of an alternative high bandgap top absorber, optimizing the current matching of the cells. However, many light management techniques tend to negatively affect the electrical and material properties of the cell. Therefore, a trade-off is established between optical and electrical performance. This paper aims to establish a balance between these two parameters in order to achieve high STH efficiencies. The final device was tested by directly connecting this cell to a Pt/IrO_x electrolyser to assess its suitability for water splitting applications.

2 | METHODS

The multijunction cell proposed is shown in Figure 1. The optimization process is divided in two main tasks. First, electrical properties were optimized by studying the different interfaces in the device. Secondly, the light management strategies were considered.

2.1 | Synthesis methods

The device structure consists on an a-Si:H/nc-Si:H/c-Si triple junction, as shown in Figure 1, where the c-Si subcell has the structure of a SHJ cell. The substrate consisted of a flat c-Si Topsil n-type <111> FZ W of approximately 280 μm, which was cleaned using a sequence of 99% HNO_3 at room temperature for 10 minutes, 69.5% HNO_3 at 100°C for 10 minutes, and 0.55% HF at room temperature for 75 seconds, with an intermediate step of deionized (DI) water after each acid step. All the thin film silicon layers were deposited using a plasma enhanced chemical vapor deposition (PECVD) multichamber system. Silane (SiH_4), hydrogen (H_2), carbon dioxide (CO_2), phosphine (PH_3), and diborane (B_2H_6) were used as precursor gases. First, two intrinsic a-Si:H layers of 7 nm were deposited on both sides of the Ws. Subsequently, 7 nm p-a-Si:H and n-a-Si:H layers were deposited on each side of the W. Then, the micromorph cell was deposited following an n-i-p sequence. The n-layer of the middle cell consisted of 30 nm of phosphorous

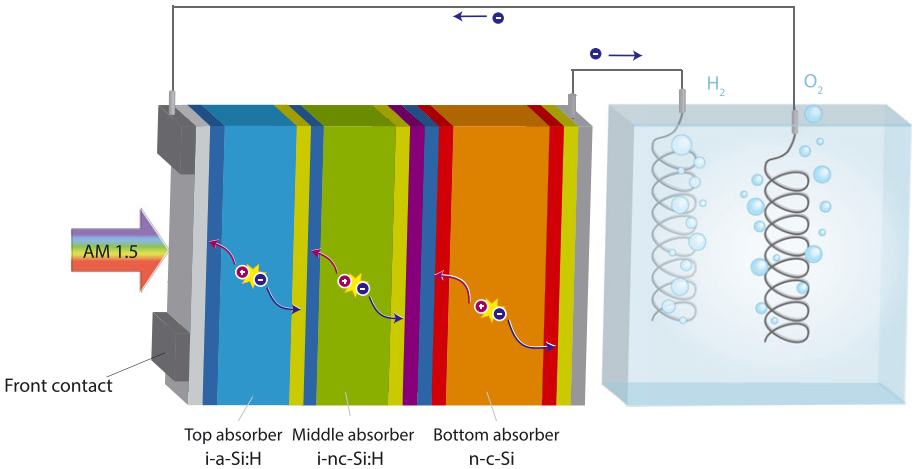

FIGURE 1 Schematic of the solar cell configuration when used for solar water splitting applications regarding supporting layers, the dark blue layers represent the p-doped layers, the yellow layers are associated to the n-doped layers, the red layers are the intrinsic amorphous silicon layer used for passivation, and the purple layer represents the different TRJs tested [Colour figure can be viewed at wileyonlinelibrary.com]

TABLE 1 External parameters of the different solar cells used in the different experiments, namely, single, double, and triple junction cells

		Substrate	V_{OC} (V)	J_{SC} Top (mA/cm^2)	J_{SC} Middle (mA/cm^2)	J_{SC} Bottom (mA/cm^2)	J_{SC} Total (mA/cm^2)	*FF* (%)	Efficiency (%)
Single junctions	a-Si:H	Flat	0.87	7.6	-	-	-	0.66	4.4
	nc-Si:H	Flat	0.51	-	17.7	-	-	0.61	5.5
	SHJ	Flat	0.69	-	-	30.7	-	0.64	13.6
Top tandem	n-SiOx:H 6 nm/a-Si:H 10 nm	Flat	1.28	11.0	7.8	-	18.8	0.57	5.7
Bottom tandem	Ref (no intermediate)	Flat	1.03	-	15.4	15.1	30.5	0.48	7.57
	n^+	Flat	1.18	-	14.8	17.8	32.6	0.54	9.68
	p^+	Flat	1.12	-	15.8	20.4	36.2	0.49	9.13
Triple junction	ITO/(p)nc-SiO$_x$:H	Flat	1.98	8.7	7.1	16.7	32.5	0.62	8.71
	IOH/(p)nc-SiO$_x$:H	Flat	1.88	9.5	8.3	17.0	34.8	0.64	9.98
	IOH/p-bilayer	Flat	2.03	9.9	8.1	16.7	34.7	0.64	10.42
	IOH/p-bilayer	Textured	1.64	10.04	9.25	16.97	36.26	0.48	7.32
	a-Si:H (H) top absorber	Flat	2.03	8.65	9.20	17.14	34.99	0.60	10.57

Abbreviations: *FF*, fill factor; IOH, hydrogenated indium oxide; ITO, indium-doped tin oxide; $J_{sc,}$ short-circuit current density; $V_{oc,}$ open-circuit voltage.

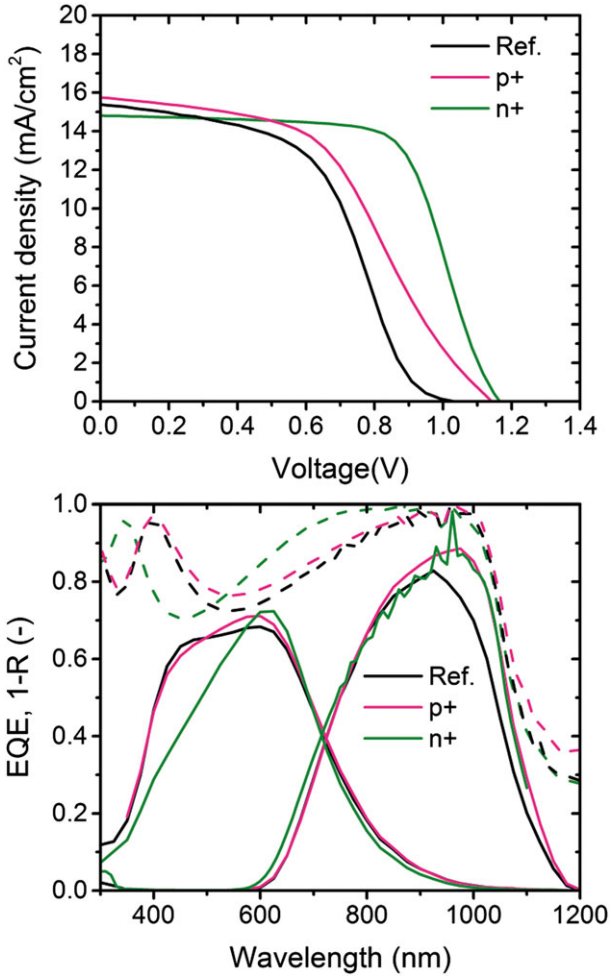

FIGURE 2 JV characteristics and external quantum efficiency (EQE) measurements of the bottom tandem deposited on flat substrates, with different doping at the tunneling recombination junctions (TRJ). The short-circuit current densities of each subcell calculated based on the EQE are summarized in Table 1 [Colour figure can be viewed at wileyonlinelibrary.com]

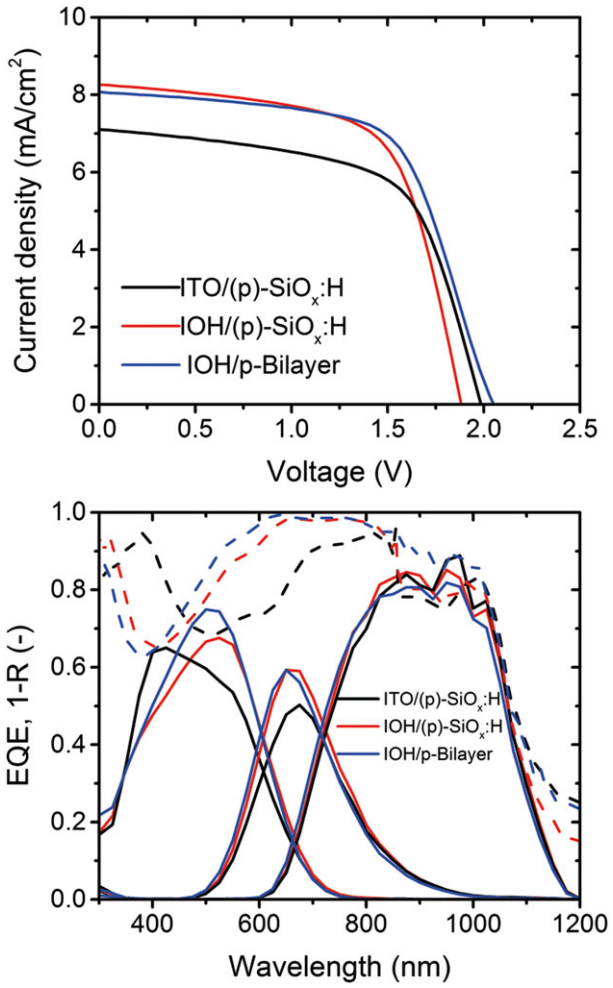

FIGURE 3 JV characteristic and external quantum efficiency (EQE) measurements of the triple junction cells deposited on flat substrates with different transparent conductive oxides (TCOs) and different top p-layer in contact with the TCO, where the p-bilayer refers to a combination of p-nc-SiO$_x$:H (8 nm) and p-nc-Si:H (4 nm) [Colour figure can be viewed at wileyonlinelibrary.com]

doped a-Si:H. The absorber layer of the middle cell consisted of 3.5 μm of nc-Si:H with a crystallinity of about 52%. The p-layer of the middle cell consisted of a boron doped nc-SiO$_x$:H. The top cell consisted of n-layer and p-layer based on nc-SiO$_x$:H, combined with an intrinsic 150 nm a-Si:H absorber layer. The highly doped layers used for TRJs were deposited by increasing the phosphine flow by 50% and the diborane flow by 100% with respect to the standard flows.

Sputtering was used to deposit the transparent conductive oxides (TCOs), both indium-doped tin oxide (ITO) and hydrogenated indium oxide (IOH). In particular, ITO was deposited as a graded layer to minimize the damage caused by ion bombardment, starting at conditions of 60°C and 0.49 W/cm^2, and increasing it to 110°C and 1.23 W/cm^2. The IOH was deposited at room temperature with a power of 1.67 W/cm^2 and 30 μbar of H_2O partial pressure, and subsequently annealed at 175°C for 150 minutes. The contacts were deposited via physical vapor deposition (PVD). The front contact consists of a grid of 500 nm Al. The back contact, which also acts as a back reflector, is formed of 200 nm Ag, 30 nm Cr, and 500 nm Al, and covers the complete back side. The cell area used was 1 cm^2. The cells have been deposited in an n-i-p configuration, but are illuminated in a p-i-n sequence.

2.2 | Characterization methods

The external quantum efficiency (EQE), defined as the percentage of photons reaching the device surface that result in collected charge carriers, was measured to further understand the current matching between the three subcells. An in-house EQE setup in TU Delft, the Netherlands, was used, consisting of a Xe lamp and a monochromator to define the wavelength range. To measure the three subcells separately, bias light of a certain wavelength was provided to saturate the other cells. The top subcell was saturated using light with wavelengths between 365 and 448 nm, the middle subcell was saturated using light between 470 and 530 nm, and the bottom subcell was saturated with light between 655 and 950 nm. The *J-V* measurements for the solar cell were obtained using a Wacom AAA solar simulator using two lamps (Xe and halogen) and an AM 1.5 filter. The current density was normalized with the short circuit current (J_{sc}) obtained from the weighted integration of the EQE measurement with respect to the AM 1.5 spectrum. The reflectance of the solar cells was measured using a Perkin Elmer Lambda 950 UV/Vis apparatus with an integrating sphere (IS). The reflectance was measured for the solar cell active area, therefore excluding the reflectance of the metal grid. To further characterize the layers, a Hitachi S4800 system was used to capture the scanning electron microscope (SEM) images of the surface and profile.

The multijunction solar cell was combined with an electrolyser based on an IrO_x anode and a Pt cathode. Both electrodes were fabricated by depositing Pt and Ir using an in-house built sputter device in TU Twente, the Netherlands. Subsequently, the EC growth of IrO_x from Ir was carried out in a 0.5 M H_2SO_4 solution with a VersaSTAT 4 potentiostat. The electrolyser was tested using a potentiostat (VersaSTAT 4) in a two-electrode configuration, where the cathode with an exposed projected surface area of 3.14 cm^2 acted as the working electrode (WE), and the anode as counter electrode (CE). Note that the WE area is bigger than the solar cell area, in order not to be limited by the active area of the catalyst. The electrolyte used was 0.5 M aqueous sulfuric acid (H_2SO_4). The light source that was used is a 300 W xenon arc light source, fitted with Air Mass filter (AM 1.5 G) from Newport, Oriel Instruments. Before every measurement, the lamp was checked by a calibrated reference solar cell (91 150 V). A steel heat sink was attached to the anode and cathode to maintain the ambient temperature stable.

3 | RESULTS AND DISCUSSION

The first step towards fabricating the proposed hybrid triple junction is to perform an electrical optimization. First, in order to assess the viability of the proposed configuration, the three separate single junctions were fabricated on a flat substrate, with the external parameters shown in Table 1. Noting the obtained individual voltages, the total sum of the open-circuit voltages is equal to 2.07 V. In addition, it is also important to realize the moderate *FF* of 0.61 for the flat nc-Si:H cell, an acceptable result considering the sensibility of nc-Si:H on the substrate texture.

In addition, the top (a-Si:H/nc-Si:H) and bottom (nc-Si:H/c-Si) tandems have been studied separately to better isolate the effects of each junction before integrating all components in a triple junction cell. The junction between the a-Si:H and nc-Si:H has been widely studied in literature,[13,14] and the concept of intermediate reflectors such as a combination of n-a-Si:H and n-nc-SiO_x:H has been shown to improve the optical and electrical properties of the tandem cell.[15,16] In this work, a combination of 6 nm n-nc-SiO_x:H/10 nm n-a-Si:H was used. Nevertheless, the bottom TRJ is the most crucial and innovative junction of this device, since it combines the difficulties of c-Si W passivation and the growth of nc-Si:H on flat surfaces, on top of all the other traditional

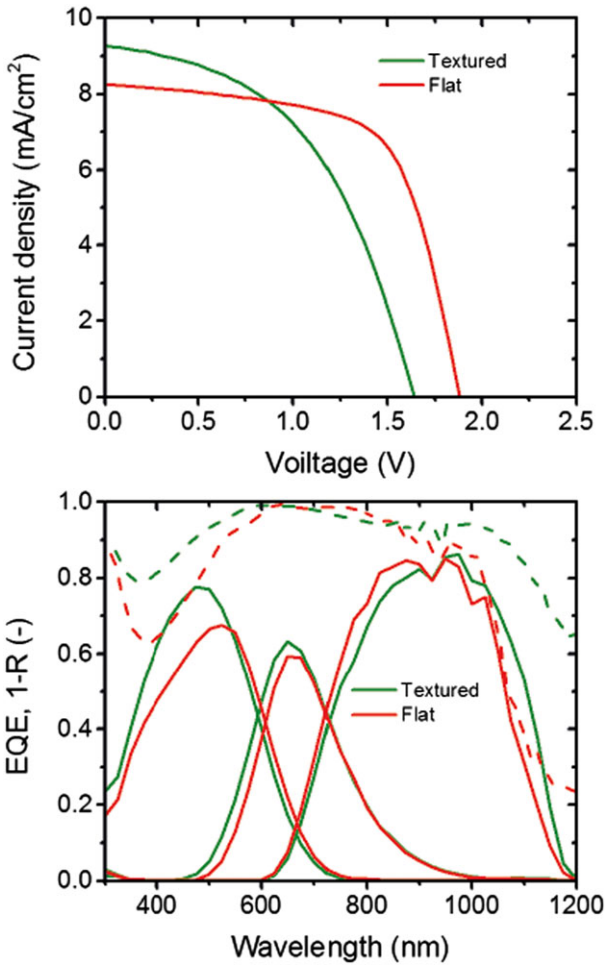

FIGURE 4 Comparison of solar cell JV characteristics and external quantum efficiency (EQE) of between flat and textured solar cells [Colour figure can be viewed at wileyonlinelibrary.com]

challenges of TRJs. The chosen approach consisted of using highly doped n-layer and p-layer (ie, n^+ and p^+, respectively) on the middle and bottom subcells, respectively. This improves tunneling by placing the conduction and valence band closer.[12] It must be noted that the highly doped p-layer cell includes a thicker (i)a-Si:H passivating layer for the SHJ subcell in order to avoid boron atom migration to the c-Si surface, and the subsequent loss in c-Si passivation.[12] Figure 2 shows the effects of including a higher p-doped and n-doped layers next to the junction. Both for the case of higher dopant concentration in the p-layer and n-layer, the performance is improved, as shown in Table 1 and Figure 2. The V_{oc} is higher when using highly doped layers. However, the *FF* is lower for the p^+ case compared with the n^+ case, indicating the introduction of high series resistance in the cell due to the thicker a-Si:H layer. The best results were obtained using higher doping in the n-layer of the nc-Si:H subcell, which does not introduce any additional resistances in the system, and at the same time, increases tunneling at the recombination interface. This can also be seen in the negligible loss of voltage when comparing the V_{oc} of this cell (1.18 V) with the maximum potential based on the single junction cells (1.20 V). However, a barrier can still be seen with regards to the series resistance, probably because of the front interface between the p-layer and the ITO, which has not been optimized. Finally, it can be seen in the EQE characteristic that for the case of a higher doped n-layer, the optical response of the top cell also varies, showing lower EQE values on the blue part of the spectrum. This might be caused by a difference in reflection and absorbance at the cell front surface due to instabilities associated with the quality and thickness of the ITO deposition. Nevertheless, since the highly doped n-layer samples show the best *FF* and V_{oc} without a major detrimental effect on the short-circuit current (J_{sc}), it is assumed to be the best choice for this TRJ, and thus it would be used further in the triple junction configuration.

Using the TRJ developed and an ITO layer as front TCO, a triple junction was fabricated, achieving a V_{oc} of 1.98 V, an FF of 0.62, a current density of 7.13 mA/cm^2, and a final efficiency of 8.71%, as shown in Figure 3 and Table 1. To further improve the efficiency, the limiting parameters must be identified. Since the V_{oc} and *FF* achieved are relatively close to the theoretically possible values as compared with the fabricated single junction cells (see Table 1), other strategies must be considered. An important factor when improving this cell is the light management. Looking at the J_{sc} values in Table 1, it becomes clear that the middle subcell is the current limiting one, and where the light management strategies would focus. The thickness of the nc-Si:H subcell was limited to 3.5 μm, since a thicker absorber layer results in a degradation of the electrical parameters of the cell. A promising strategy is to vary the front TCO, which is responsible for a large amount of reflection at the cell surface, as seen in the 1-R depicted in Figure 3. ITO was replaced by a more transparent and conductive IOH, which would avoid high reflection in the region between 500 and 900 nm, and thus would allow for more light to reach the middle cell. By using IOH, a V_{oc} of 1.88 V was achieved, with an *FF* of 0.64, a current density of 8.28 mA/cm^2, and a final efficiency of 9.98%, as shown in Table 1.

Since the IOH layer improved the light management but decreased the open circuit voltage, further experiments were conducted regarding the contact between the front p-layer and the TCO. To improve the contact at the front surface, a p-doped nanocrystalline silicon thin layer is placed between the p-layer and the IOH layer, followed by an H_2 treatment to passivate any dangling bonds. This could potentially lower

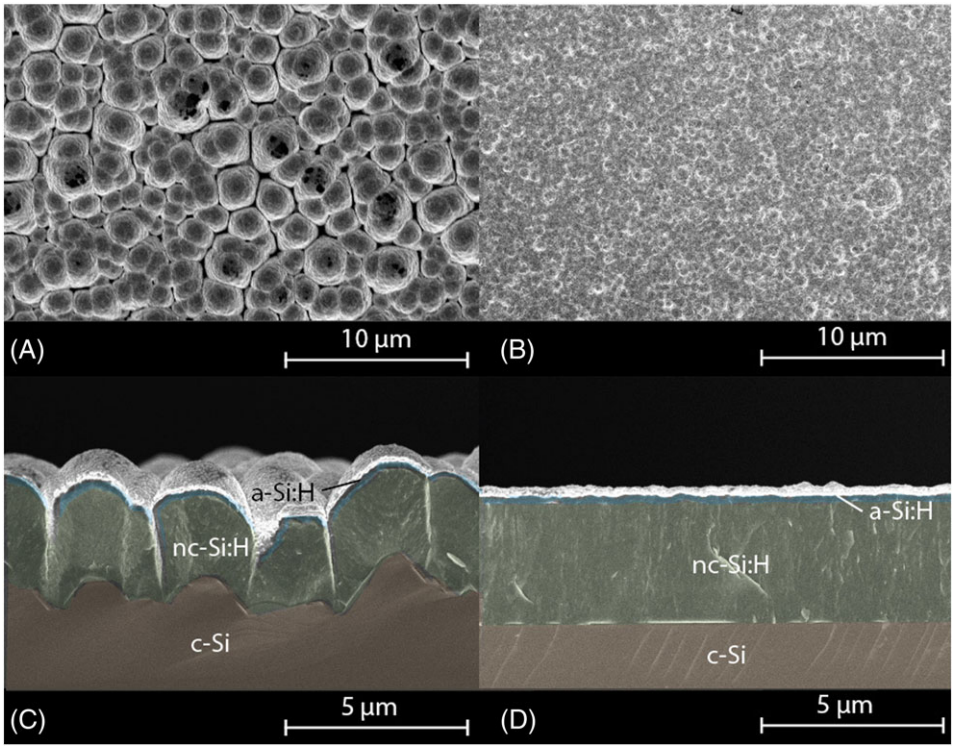

FIGURE 5 Scanning electron microscope (SEM) top view and profile of a textured (A, C) and flat (B, D) solar cells [Colour figure can be viewed at wileyonlinelibrary.com]

the energy barrier at the interface between p-layer and TCO,[34] since nc-Si:H materials are able to achieve a lower activation energy (51.3 meV) than the p-SiO_x:H material previously used (240.9 meV). The open circuit voltage achieved when including the p-bilayer at the front is 2.03 V. This strategy also increases the series and shunt resistances, resulting in a similar *FF* of 0.64 and a PV conversion efficiency of 10.47%. Interestingly, looking at the EQE measurements in Figure 3 and Table 1, it seems that there is also a slight improvement in the optical performance of the top cell at low wavelengths, while the EQE of the other two subcells slightly decreases. Even though this does not affect the overall performance of the cell, since it is limited by the middle cell, this change is interesting. Introducing a p-bilayer with different refractive indexes can reduce the reflection at the front surface of the cell (refractive index grading), increasing the overall performance. Most importantly, the electrical properties are improved by facilitating the charge carrier injection from the solar cell into the TCO, suggesting that an IOH/p-bilayer configuration is beneficial to fabricate an efficient triple junction cell.

With these improvements, the V_{oc} of the triple junction solar cell (2.03 V) is very close to the sum of the voltages produced by the single junction cells (2.07 V). The *FF* of 0.64 is also comparable with the single junction cells (Table 1), suggesting that the tunneling recombination junctions are not the main factor limiting the electrical properties of this cell. Instead, it is speculated that the bulk of the nc-Si:H subcell is the main cause of FF loss. However, by comparing the short-circuit currents of the subcells in Table 1, a great current mismatch can be observed, with the middle cell being the limiting factor. This suggests that further light management techniques are needed to achieve current matching and higher spectral utilization. One of the most challenging aspects of building this multijunction cell is the growth of the nc-Si:H subcell. This material does not grow well on flat surfaces because of internal stresses leading to cracks and poor adhesion to the substrate.[6,17,18] This study explores how texture can affect the performance of the triple junction cells.

When comparing the performance of the cells deposited on textured and flat substrates, there seems to be a trade-off between the current density, the open circuit voltage, and the *FF*, as shown in Figure 4. The textured cells are able to achieve better current densities due to better light management, especially in the blue wavelength range, as seen in the EQE in Figure 4. In addition, the reflectance is significantly reduced for both short and long wavelengths, and the short circuit current achieved by the textured W is 9.25 mA/cm^2, as opposed to the 8.28 mA/cm^2 obtained by the flat device. Finally, the adhesion of the cells to the crystalline silicon W that acts as a substrate is improved, since the internal stresses in the nc-Si:H layer are reduced. However, there is a significant loss in the V_{oc} and *FF* when the W is textured, as shown in Figure 4 and Table 1. In particular, the V_{oc} drops from 1.88 to 1.65 V, and the *FF* is reduced from 0.64 to only 0.48. This is expected to be because of shunts that appear in the nc-Si:H and a-Si:H structures when the texture features are too sharp.[35] These losses would finally cause a reduction in overall PV conversion efficiency of −2.66% absolute, from 9.98% to 7.32%.

To confirm the effect of the textured W on the nc-Si:H growth, SEM measurements have been performed, as shown in Figure 5. The top view of the textured samples show much bigger, and sometimes disconnected crystals. This is confirmed when looking at the profile view, where the cracks and shunts in the nc-Si:H layer are clearly visible, as opposed to the smooth and relatively crack-free layer of the flat device. This would explain the low shunt resistance observed for the textured device in Figure 4. Moreover, the slightly higher series resistance of the textured device could also be related to the big grain boundaries and cracks, which can cause some disconnected areas in the TCO layer. Smoother textures on the c-Si W could result in less cracks, and thus better *FF* and V_{oc}, as shown by Kirner et al.[19] However, such optimization is work in progress, and thus further experiments in this paper will be performed on a flat device.

To further optimize the cell, the top a-Si:H subcell light absorption needs to be considered. By reducing the light absorption of the top subcell, the middle cell would receive more light, and the multijunction cell would be better current matched. In order to do so, the 150 nm a-Si:H top absorber can be changed by a higher bandgap a-Si:H material previously developed,[10,20-22] using higher hydrogen dilution and lower temperatures. In addition, the absorber thicknesses had to be reoptimized for the new material. The optimum thickness for the high bandgap a-Si:H is 175 nm, slightly higher than for the lower bandgap material. The comparison between the low (L) a-Si:H bandgap

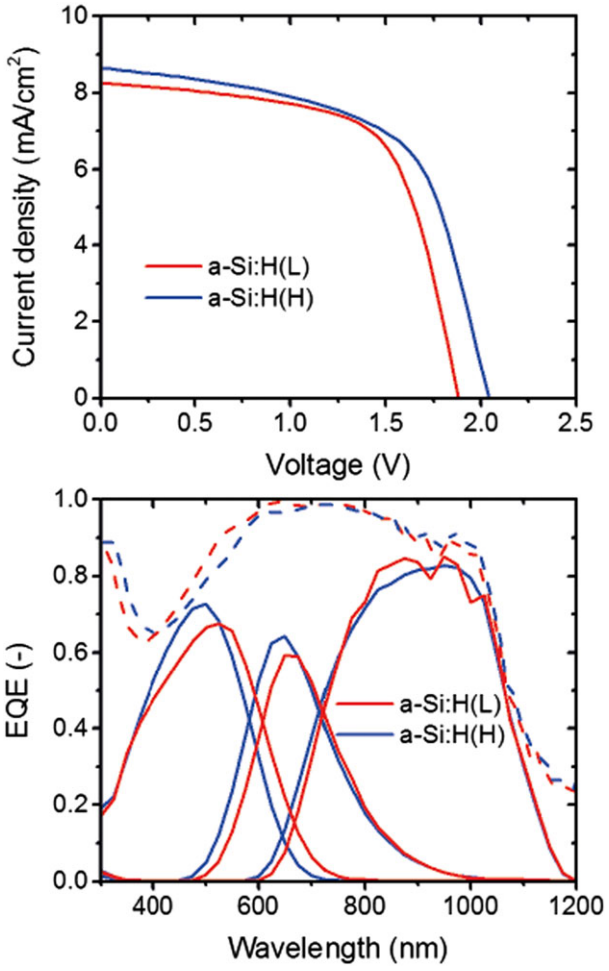

FIGURE 6 Solar cell JV characteristics and external quantum efficiency (EQE) of flat cells with a high bandgap a-Si:H top cell of different thicknesses [Colour figure can be viewed at wileyonlinelibrary.com]

(1.65 eV) and high (H) a-Si:H bandgap (1.72 eV) can be seen in Figure 6 and Table 1. The change in bandgap resulted in a higher J_{sc} compared with the reference cell. Moreover, since the material bandgap of the top absorber is slightly higher, the resulting voltage is slightly increased from 1.88 to 2.03 V. However, compared with the previous multijunction cell with a lower bandgap absorber material, with an *FF* of 0.64, this cell has a lower *FF* of 0.60, especially considering the lower shunt resistance. This can either be because of a lower material quality or because of the better current matching. Nevertheless, the overall efficiency increased from 9.98% to 10.57%, and thus, it is the chosen configuration for driving the water splitting reaction.

To further analyze the suitability of the developed triple junction solar cell for water splitting, the final device was attached to a Pt/IrOx electrolyser. The JV characteristics of both the solar cell and the electrolyser are shown in Figure 7, where the intersecting point between the two JV characteristics would be the operational point of the overall device. According to this comparison, the operational point would have a voltage of 1.65 V, close to the maximum power point (MPP) of the solar cell at 1.56 V, indicated by the square dot in the JV curve. This corresponds to a power loss of approximately 0.25 mW/cm^2 with respect to the MPP. When the device was tested for stability, a relatively constant current density was achieved for the 10 hours of measurement, changing only from 6.9 to 6.7 mA/cm^2. The resulting STH efficiency is 8.3%. To further increase this efficiency, the *FF* must be increased to achieve a better fitting between the MPP of the solar cell and the operational point of the water splitting device. This can be achieved by improving the absorber material quality of the thin film subcells.

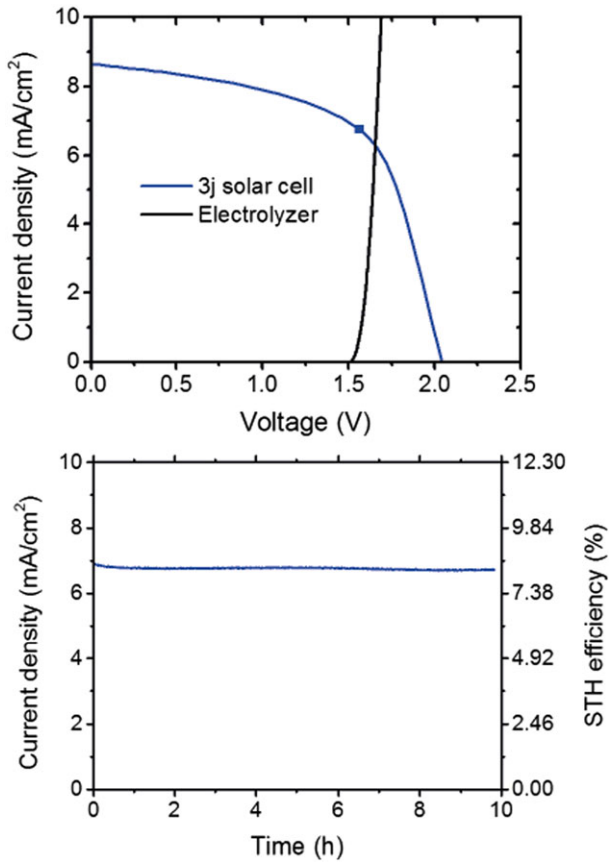

FIGURE 7 JV characteristic of the best solar cell compared with the JV characteristic of the electrolyser, and the corresponding stability characteristic of the complete system. The maximum power point of the solar cell is indicated in the JV characteristic by a square dot. Note that the current density at the intersection of the JV curves is slightly lower than the operational current recorded during the chronoamperometry tests. This is caused by minor differences in the solar simulators used [Colour figure can be viewed at wileyonlinelibrary.com]

4 | CONCLUSIONS

We propose a triple junction heterostructure consisting of a-Si:H (TF)/nc-Si:H (TF)/c-Si(W) in order to achieve the desired voltages for solar water splitting, between 1.6 and 2 V. The main two challenges tackled in this paper include the development of TRJs for this device and the application of light management techniques. The optimum top TRJ considered was based on 6 nm of n-nc-SiO$_x$:H and 10 nm n-nc-Si:H, whereas the bottom TRJ is enhanced by increasing the doping on the middle subcell n-layer. This allows for efficient charge carrier collection within the cell, while enhancing the recombination at the interface between each subcell to maintain current continuity. In order to further improve the solar cell efficiency, light management techniques are applied. The resulting multijunction cell performance is limited by the current density of the middle cell. This can be improved by using IOH as TCO, which allows for higher absorption in the middle subcell. A combination of p-nc-Si:H and p-nc-SiO$_x$:H at the front surface was then necessary to create a good electric contact of the cell to the front TCO. Another light management technique considered is substrate texturing. Although conventional W texturing can achieve higher current densities due to light trapping and antireflection effects, the sharpness on the features creates cracks and short circuits in the nc-Si:H absorber layer, resulting in an overall reduced V_{oc}, *FF*, and efficiency. Alternative textures and processes that avoid those cracks must be explored, and are currently work in progress. For the purpose of this paper, flat Ws are chosen as the preferred solution. Finally, to improve the current matching, a top absorber a-Si:H with a slightly higher bandgap energy was introduced. The device including this top absorber achieved a PV efficiency of 10.57%, with an *FF* of 0.60, a V_{oc} of 2.03 V, and a short-circuit current density of 8.65 mA/cm^2. When connected to a Pt/IrO$_x$ electrolyser, an STH efficiency of 8.3% was achieved. The performance was stable for 10 hours of measurement.

5 | OUTLOOK

This paper presents the development of a hybrid silicon based solar cell for water splitting applications and demonstrates an efficiency of 8.3%. To put these results into context, a brief review of the solar water splitting field is presented. Moreover, the developed device will be compared with the most efficient systems developed.

As already briefly mentioned, the proposed approach is not the only one for solar water splitting. Different materials and configurations can be used besides a silicon multijunction. Some of the most important concepts are depicted in Figure 8, placed in a scale of a completely monolithically integrated device (A) to a completely decoupled one (E). All of these concepts have their advantages and disadvantages.

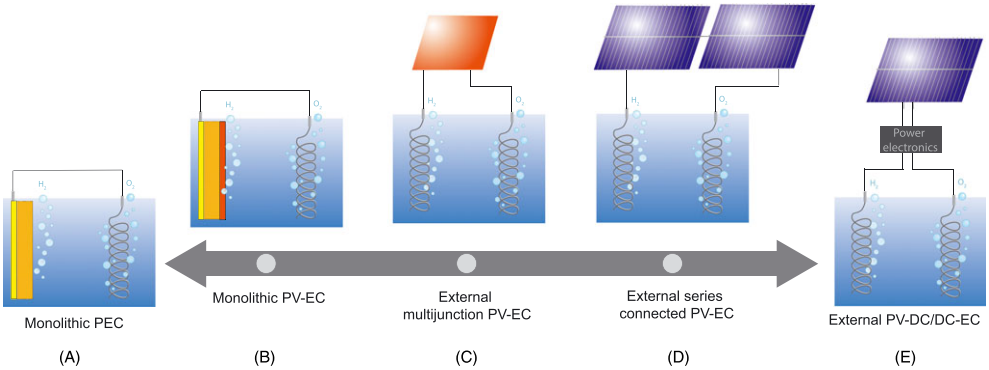

FIGURE 8 Scale of the different possible solar water splitting devices, from the monolithical phototelectrochemical (PEC) devices A, where the two aspects are completely coupled; to a PV-DC/DC-EC system E, where the two elements are completely decoupled by a DC/DC converter. Some examples of intermediate devices include monolithical photovoltaic-electrochemical device (PV-EC) devices B, which refers to a buried photovoltaic (PV) junction directly in contact with water; external multijunction PV-EC devices C, where the PV cell is outside the electrolyte, but it still produces enough voltage by itself for the electrolysis reaction; and external series connected PV-EC devices D, where several cells are connected in series to produce the required voltage, but it does not include any additional electronic components [Colour figure can be viewed at wileyonlinelibrary.com]

Several materials have been tested as photoelectrode for the realization of a photoelectrochemical (PEC) device as shown in configuration (A),[23,24] including[25,26] TiO_2, α-Fe_2O_3, WO_3, III-V technologies,[27] or[28] $BiVO_4$. However, previous research suggests the need for a buried PV junction to separate and collect the charge carriers at the semiconductor/electrolyte interface more efficiently, preventing Fermi level pinning.[29] A buried PV junction relaxes the conditions and design considerations of the semiconductor device.[30,31] In addition, very few of these materials have a high enough bandgap to provide the voltage needed for the reaction without an external bias.[32,33] That is why several series connected PV cells are needed, which can be accomplished by many different configurations, as shown in Figure 8.

Two of the most promising designs are to externally connect several cells in series (D) and to fabricate a monolithic device to produce the necessary voltage and current (B, C). External series connected photovoltaic-electrochemical device (PV-EC) devices (D) have the advantage of taking readily available devices to achieve high efficiencies, as shown in literature with three heterojunction cells combined with an earth-abundant material electrolyser resulting in an efficiency[34] of 14.2%. In addition, it can result in a better current matching, especially at variable spectrum conditions, since all the cells would be of the same technology and would produce similar current densities at a certain spectrum. On the other hand, PV-EC devices (B, C) have the advantage of an overall better spectral utilization, and possibly lower losses due to less cabling. In addition, since cell interconnections can be avoided, the final device could be more compact and easily produced, lowering the cost of these devices. When comparing the designs (B) and (C), configuration (B) might need additional protective layers to be able to operate in contact with the electrolyte, which can cause additional losses and reduce the lifetime of the complete device. STH efficiencies[35] of 18.3% have been demonstrated with concentrated light and a III-V/c-Si multijunction device,[36] and up to 19.3% with purely III-V multifunctions.[37] However, III-V materials are not economically feasible in large scale because of their scarcity and associated high cost. Therefore, there is a need for devices based on earth-abundant materials that can efficiently split water, such as silicon. TF silicon devices are widely known for their application in solar cells for electricity generation.[38,39] They have also been previously tested for solar water splitting. Rocheleau et al[40] reported a 7.8% STH efficiency using a triple junction amorphous silicon solar cell combined with a catalytic Ni/$NiFe_yO_x$ electrode. Nevertheless, TF cells have limited light absorption. To overcome the light management limitations of purely TF devices while still being cost-effective, some hybrid approaches have been proposed. Monolithic perovskite/c-Si cells have previously reported efficiencies of 23.6% as PV devices.[41] However, the crucial shortcomings of these structures are the relatively low stability, especially in the presence of water, and the use of lead in the structure.[42] To have a more clear picture of how the different technologies compare, the highest achieved efficiencies both as PV and for hydrogen generation purposes (STH efficiency) have been plotted in Figure 9.

Although the proposed hybrid device consisting on a a-Si:H/nc-Si:H/c-Si multijunction presents the lowest efficiency of all the results plotted, it must be noted that we are comparing a new concept with mature technologies such as SHJ or III-V technologies. Nevertheless, the obtained results are still close to the ones achieved for TF multijunctions. Moreover, it must be noted that the concept developed in this paper shows the smallest differences between PV and STH efficiencies, confirming its suitability to be applied for solar water splitting. Finally, it must also be noted that Figure 9 does not show the availability, toxicity, or stability of these materials. If these elements are considered, the developed device can be considered even more suitable for further industrialization since it is based on silicon and is relatively stable when compared with other technologies such as perovskites. To reach such scale, further improvements in the material quality and light trapping strategies must be implemented to reach efficiencies comparable with those presented in Figure 9.

Finally, a completely decoupled system could be designed (E), where the working conditions of the PV device do not depend on the EC component due to the DC/DC converter installed in between

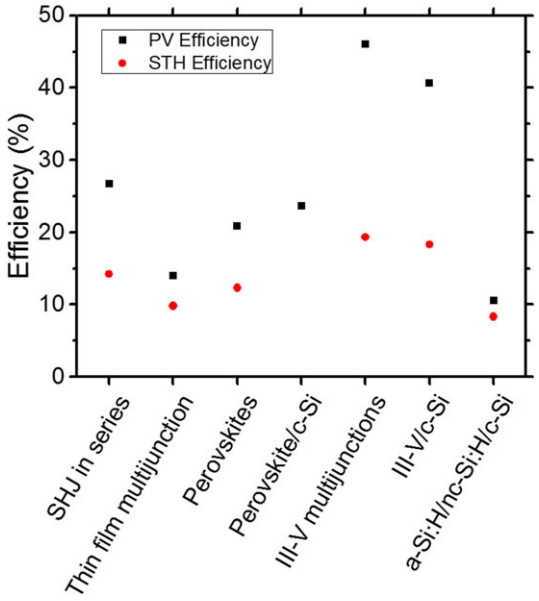

FIGURE 9 Comparison of the highest achieved efficiencies both as photovoltaic (PV) and solar-to-hydrogen (STH). (PV data collected from the study of Green,[43] STH data collected from the studies of Ager and Luo et al[44,45] [Colour figure can be viewed at wileyonlinelibrary.com]

them. Since all these technologies are relatively mature, a 20.6% STH efficiency was achieved, and a potential of 26.5% was simulated as a theoretical limit.[46] However, it must be noticed that these approaches (E) have an increasing complexity, and thus achieving a similar efficiency with simpler, more compact devices (B, C) can be more cost-effective.

ACKNOWLEDGEMENTS

The authors thank Johan Blanker for his help regarding the SEM measurements and Dr Paul Procel Moya for providing the textured wafers. This work is part of the research program of the Foundation for Fundamental Research on Matter (FOM-13CO19), which is part of the Netherlands Organization for Scientific Research (NWO).

ORCID

Paula Perez-Rodriguez http://orcid.org/0000-0002-2188-9705

REFERENCES

1. Nicoletti G, Arcuri N, Nicoletti G, Bruno R. A technical and environmental comparison between hydrogen and some fossil fuels. *Energ Conver Manage*. 2015;89:205-213.
2. Fountaine KT, Lewerenz HJ, Atwater HA. Efficiency limits for photoelectrochemical water-splitting. *Nat Commun*. 2016;7:13706.
3. Calvet W, Murugasen E, Klett J, et al. Silicon based tandem cells: Novel photocathodes for hydrogen production. *Phys Chem Chem Phys*. 2014;16(24):12043-12050.
4. Fang J, Ren Q, Wang F, et al. Amorphous silicon/crystal silicon heterojunction double-junction tandem solar cell with open-circuit voltage above 1.5 V and high short-circuit current density. *Sol Energy Mater Sol Cells*. 2018;185:307-311.
5. Kirner S. Wafer surface tuning for a-Si:H/nc-Si:H/c-Si triple junction solar cells for application in water splitting. *Energy Procedia*. 2016;102:126-135.
6. Agbo SN. Growth and characterization of thin film nanocrystalline silicon materials and solar cells. Delft, The Netherlands, Delft University of Technology. PhD; 2012.
7. Roschek T, Rech B, Beyer W, et al. Microcrystalline silicon solar cells prepared by 13.56 MHz PECVD at high growth rates: Solar cell and material properties. *MRS Proceedings*. 2001;664:A25.5.1. https://doi.org/10.1557/PROC-664-A25.5.1
8. Bills B, Liao X, Galipeau DW, Fan QH. Effect of tunnel recombination junction on crossover between the dark and illuminated current-voltage curves of tandem solar cells. *IEEE Trans Electron Devices*. 2012;59(9):2327-2330.
9. Chang P-K, Lu C-H, Yeh C-H, Houng M-P. High efficiency a-Si:H/a-Si:H solar cell with a tunnel recombination junction and a n-type uc-Si:H layer. *Thin Solid Films*. 2012;520(9):3684-3687.
10. Si FT, Isabella O, Tan H, Zeman M. Quadruple-junction thin-film silicon solar cells using four different absorber materials. *Solar RRL*. 2017;1(3–4):1700036.
11. Lee Y, Dao VA, Iftiquar SM, Kim S, Yi J. Current transport studies of amorphous n/p junctions and its application in a-Si:H/HIT-type tandem cells. *Prog Photovolt Res Appl*. 2016;24:52-58. https://doi.org/10.1002/pip.2644
12. Vasudevan R, Thanawala Z, Han L, et al. A thin-film silicon/silicon hetero-junction hybrid solar cell for photoelectrochemical water-reduction applications. *Sol Energy Mater Sol Cells*. 2016;150:82-87.
13. Buehlmann P, Bailat J, Dominé D, et al. In situ silicon oxide based intermediate reflector for thin-film silicon micromorph solar cells. *Appl Phys Lett*. 2007;91(143505):1-3.
14. Yan B, Yue G, Sivec L, Yang J, Guha S, Jiang CS. Innovative dual function nc-SiOx:H layer leading to a >16% efficient multi-junction thin-film silicon solar cell. *Appl Phys Lett*. 2011;99(11):113512.
15. Bielawny A, Üpping J, Miclea PT, et al. 3D photonic crystal intermediate reflector for micromorph thin-film tandem solar cell. *Physica Status Solidi*. 2008;205(12):2796-2810.
16. Söderström T, Haug FJ, Niquille X, Terrazzoni V, Ballif C. Asymmetric intermediate reflector for tandem micromorph thin film silicon solar cells. *Appl Phys Lett*. 2009;94(6):063501.
17. Roschek T, Rech B, Beyer W, et al. Microcrystalline silicon solar cells prepared by 13.56 MHz PECVD at high growth rates: Solar cell and material properties. *Symp A—Amorphous Heterog Silicon-Based Films-2001*. 2001;664:A25.25.21.
18. Tan H, Babal P, Zeman M, Smets AHM. Wide bandgap p-type nanocrystalline silicon oxide as window layer for high performance thin-film silicon multi-junction solar cells. *Sol Energy Mater Sol Cells*. 2015;132:597-605.
19. Kirner S, Sarajan H, Azarpira A, et al. Wafer surface tuning for a-Si:H/µc-Si:H/c-Si triple junction solar cells for application in water splitting. *Energy Procedia*. 2016;102:126-135.
20. Fischer M, Tan H, Melskens J, Vasudevan R, Zeman M, Smets AHM. High pressure processing of hydrogenated amorphous silicon solar cells: Relation between nanostructure and high open-circuit voltage. *Appl Phys Lett*. 2015;106(4):043905.
21. Smets AHM, Wank MA, Vet B, et al. The relation between the bandgap and the anisotropic nature of hydrogenated amorphous silicon. *IEEE J Photovoltaics*. 2012;2(2):94-98.
22. Tan H, Moulin E, Si FT, et al. Highly transparent modulated surface textured front electrodes for high-efficiency multijunction thin-film silicon solar cells. *Prog Photovolt Res Appl*. 2015;23(8):949-963.
23. Fujishima A, Honda K-I, Kikuchi S-I. Photosensitized electrolytic oxidation on semiconduction n-type TiO2 electrode. *J Soc Chem Ind, Japan*. 1969;72(1):108-113.
24. Hwang Y, Hahn C, Liu B, Yang P. Photoelectrochemical properties of TiO2 nanowire arrays: A study of the dependence on length and atomic layer deposition coating. *ACS Nano*. 2012;6(6):5060-5069.
25. Bassi PS, Gurudayal, Wong LH, Barber J. Iron based photoanodes for solar fuel production. *Phys Chem Chem Phys*. 2014;16(24):11834-11842.

26. Dotan H, Sivula K, Gratzel M, Rothschild A, Warren S. Probing the photoelectrochemical properties of hematite (a-Fe2O3) electrodes using hydrogen peroxide as a hole scavenger. *Energy Environ Sci*. 2011;4(3):958-964.
27. Malizia M, Seger B, Chorkendorff I, Vesborg PCK. Formation of a p-n heterojunction on GaP photocathodes for H2 production providing an open-circuit voltage of 710 mV. *J Mater Chem A*. 2014;2(19):6847-6853.
28. Abdi FF. Efficient BiVO4 photoanodes thin film modified with cobalt phosphate catalyst and W-doping. *Chem Cat Chem*. 2013;5:490-496.
29. Han L, Abdi FF, van de Krol R, et al. Efficient water-splitting device based on a bismuth vanadate photoanode and thin-Film silicon solar Cell. *ChemSusChem*. 2014;7(10):2832-2838.
30. Cox C, Winkler MT, Pijpers JJH, Buonassisi T, Nocera DG. Interfaces between water splitting catalysts and buried silicon junctions. *Energ Environ Sci*. 2013;6(2):532-538.
31. Seger B, Pedersen T, Laursen AB, Vesborg PCK, Hansen O, Chorkendorff I. Using TiO2 as a conductive protective layer for cathodic H2 evolution. *J Am Chem Soc*. 2013;135(3):1057-1064.
32. Hu S, Xiang C, Haussener S, Berger AD, Lewis NS. An analysis of the optimal band gaps of light absorbers in integrated tandem photoelectrochemical water-splitting systems. *Energ Environ Sci*. 2013;6(10):2984-2993.
33. van de Krol R, Grätzel M. *Photoelecrochemical Hydrogen Production*. Springer; 2012. ISBN 978-1-4614-1380-6
34. Schuttauf J-W, Modestino MA, Chinello E, et al. Solar-to-hydrogen production at 14.2% efficiency with silicon photovoltaics and earth-abundant electrocatalysts. *J Electrochem Soc*. 2016;163(10):F1177-F1181.
35. Licht S, Wang B, Mukerji S, Soga T, Umeno M, Tributsch H. Efficient solar water splitting exemplified by RuO2-catalyzed AlGaAs/Si photoelectrolysis. *J Phys Chem B*. 2000;104(38):8920-8924.
36. Khaselev O, Bansal A, Turner JA. High-efficiency integrated multijunction photovoltaic/electrolysis system for hydrogen production. *Int J Hydrogen Energy*. 2001;26(2):127-132.
37. Cheng W-H, Richter MH, May MM, et al. Monolithic photoelectrochemical device for direct water splitting with 19% efficiency. *ACS Energy Letters*. 2018;3(8):1795-1800.
38. Mohr N, Meijer A, Huijbregts MAJ, Reijnders L. Environmental life cycle assessment of roof-integrated flexible amorphous silicon/nanocrystalline silicon solar cell laminate. *Prog Photovolt Res Appl*. 2013;21(4):802-815.
39. Terakawa A. Review of thin-film silicon deposition techniques for high-efficiency solar cells developed at Panasonic/Sanyo. *Sol Energy Mater Sol Cells*. 2013;119:204-208.
40. Rocheleau R, Miller EL, Misra A. High-efficiency photoelectrochemical hydrogen production using multijunction amorphous silicon photoelectrodes. *Energy Fuel*. 1998;12(1):3-10.
41. Bush K, Palmstrom AF, Yu ZJ, et al. 23.6%-efficient monolithic perovskite/silicon tandem solar cells with improved stability. *Nature Energy*. 2017;2(4):17009.
42. Essig S, Allebé C, Remo T, et al. Raising the one-sun conversion efficiency of III-V/Si solar cells to 32.8% for two junctions and 35.9% for three juntions. *Nature Energy*. 2017;2(9):17144.
43. Green MA, Hishikawa Y, Dunlop ED, Levi DH, Hohl-Ebinger J, Ho-Baillie AWY. Solar cell efficiency tables (version 51). *Prog Photovolt Res Appl*. 2018;26:3–12. https://doi.org/10.1002/pip.2978
44. Ager J. Experimental demonstrations of spontaneous, solar-driven photoelectrochemical water splitting. *Energ Environ Sci*. 2015;8(10):2811-2824.
45. Luo J, Im JH, Mayer MT, et al. Water photolysis at 12.3% efficiency via perovskite photovoltaics and earth-abundant catalysts. *Science*. 2014;345(6204):1593-1596.
46. Chang WJ, Lee KH, Ha H, et al. Design principle and loss engineering for photovoltaic–electrolysis cell system. *ACS Omega*. 2017;2(3):1009-1018.

How to cite this article: Perez-Rodriguez P, Vijselaar W, Huskens J, et al. Designing a hybrid thin-film/wafer silicon triple photovoltaic junction for solar water splitting. *Prog Photovolt Res Appl*. 2018;1–10. https://doi.org/10.1002/pip.3085